

# ROMNet: Renovate the Old Memories

Runsheng Xu<sup>†</sup>, Zhengzhong Tu<sup>†</sup>, Yuanqi Du<sup>†</sup>, Xiaoyu Dong, Jinlong Li, Zibo Meng, *Member, IEEE*,  
Jiaqi Ma\*, Hongkai Yu\*, *Member, IEEE*

**Abstract**—Renovating the memories in old photos is an intriguing research topic in computer vision fields. These legacy images often suffer from severe and commingled degradations such as cracks, noise, and color-fading, while lack of large-scale paired old photo datasets makes this restoration task very challenging. In this work, we present a novel reference-based end-to-end learning framework that can jointly repair and colorize the degraded legacy pictures. Specifically, the proposed framework consists of three modules: a restoration sub-network for degradation restoration, a similarity sub-network for color histogram matching and transfer, and a colorization subnet that learns to predict the chroma elements of the images conditioned on chromatic reference signals. The whole system takes advantage of the color histogram priors in a given reference image, which vastly reduces the dependency on large-scale training data. Apart from the proposed method, we also create, to our knowledge, the first public and real-world old photo dataset with paired ground truth for evaluating old photo restoration models, wherein each old photo is paired with a manually restored pristine image by PhotoShop experts. Our extensive experiments conducted on both synthetic and real-world datasets demonstrate that our method significantly outperforms state-of-the-arts both quantitatively and qualitatively.

**Index Terms**—Image restoration, image colorization, old photo restoration, image enhancement, histogram fusion

## I. INTRODUCTION

WHILE everything stays colorful in our old memories, they are generally stored as gray-scale legacy photos. As time elapsed, they also suffer from various types of degradation. Experts have put extensive efforts into image restoration and colorization to make the old memories alive again during the past decades. However, manually doing these requires expertise in both computer vision and Photoshop techniques, making it labor-intensive and time-consuming. Thus, developing automatic systems for picture colorization and restoration is a problem of pressing interest.

With emerging deep learning techniques, image restoration and colorization have achieved a higher level of performance. Deep learning-based approaches have been widely studied and demonstrated promising for degraded image restoration and enhancement, such as image denoising [1], [2], super-resolution [3], [4], deblurring [5], [6], and compression [7], [8]. In terms of applying deep learning in image colorization,

it generally demands large-scale data for training [9] to achieve favorable performance. However, training a deep network using large-scale datasets (e.g., on ImageNet [10]) is energy-inefficient and time-consuming. Moreover, preparing the large-scale dataset is usually labor expensive. To deal with these problems, previous works [11]–[14] proposed to employ reference/example images to assist image colorization on gray-scale images. He *et al.* [13] fuses the raw AB channel of the reference image’s LAB color space to colorize the grayscale image. But as [15] pointed out, there is inherent ambiguity in the color of natural objects, and directly providing the certain pixel value will ignore the statistical color distribution and break such ambiguity. Yoo *et al.* [16] uses the mean and variance of extracted deep color features as guidance, however it ignores the spatial information in the transfer, and thus discards the implicit correlation information between texture and color.

Given that the statistical color distribution and the spatial information are both useful for colorization, we propose a reference-based multi-scale spatial-preserving color histogram fusion method for image colorization, where the use of a reference image to colorize the gray-scale image helps us to get rid of the curse of large-scale training data. Precisely, we devise a novel end-to-end deep learning framework for old photo restoration, dubbed **ROMNet** (**R**enovate the **O**ld **M**emories), which is composed of 1) a convolutional sub-network for degradation restoration, 2) a similarity sub-network for reference color matching, and 3) a colorization sub-network to render the final colorful image. As illustrated in Fig. 1, ROMNet is capable of restoring and colorizing the degraded old photos with limited training data, making it attractive for data-efficient applications. Previous methods [17] mainly use the quantitative results on synthetic data with the restoration ground truth and qualitative results on collected real data without the restoration ground truth for the experimental evaluation. To the best of our knowledge, there is no real-world public dataset with the restoration and colorization ground truth in this research area. To push forward the research interests in this area, we build the *first real-world old photo dataset* (200 authentic grayscale old photos), where each old photo is paired with a ‘pristine’ image manually restored and colorized by Adobe Photoshop experts. Our experimental results show that ROMNet, even with a smaller training set, outperforms the state-of-the-art methods on both publicized synthetic dataset and our real-world old photo dataset.

The major contributions of this paper are summarized as follows:

- We propose the *first end-to-end deep learning framework* (ROMNet) which learns to jointly restore and colorize the degraded old photos requiring only a limited amount of

Runsheng Xu and Jiaqi Ma are with UCLA Mobility Lab, University of California, Los Angeles, CA, 90095, USA. Runsheng Xu is also with Cleveland State University, Cleveland, OH, 44115, USA. Zhengzhong Tu is with University of Texas at Austin, Austin, TX, 78712, USA. Yuanqi Du is with George Mason University, Fairfax, VA, 22030, USA. Xiaoyu Dong is with Northwestern University, Evanston, IL, 60208, USA. Zibo Meng is with Innopack Technology, Palo Alto, CA, 94303, USA. Jinlong Li and Hongkai Yu are with Cleveland State University, Cleveland, OH, 44115, USA.

<sup>†</sup> The first three authors contributed equally to this work.

\* Corresponding authors: Jiaqi Ma (e-mail: jiaqima@ucla.edu) and Hongkai Yu (e-mail: h.yu19@csuohio.edu).

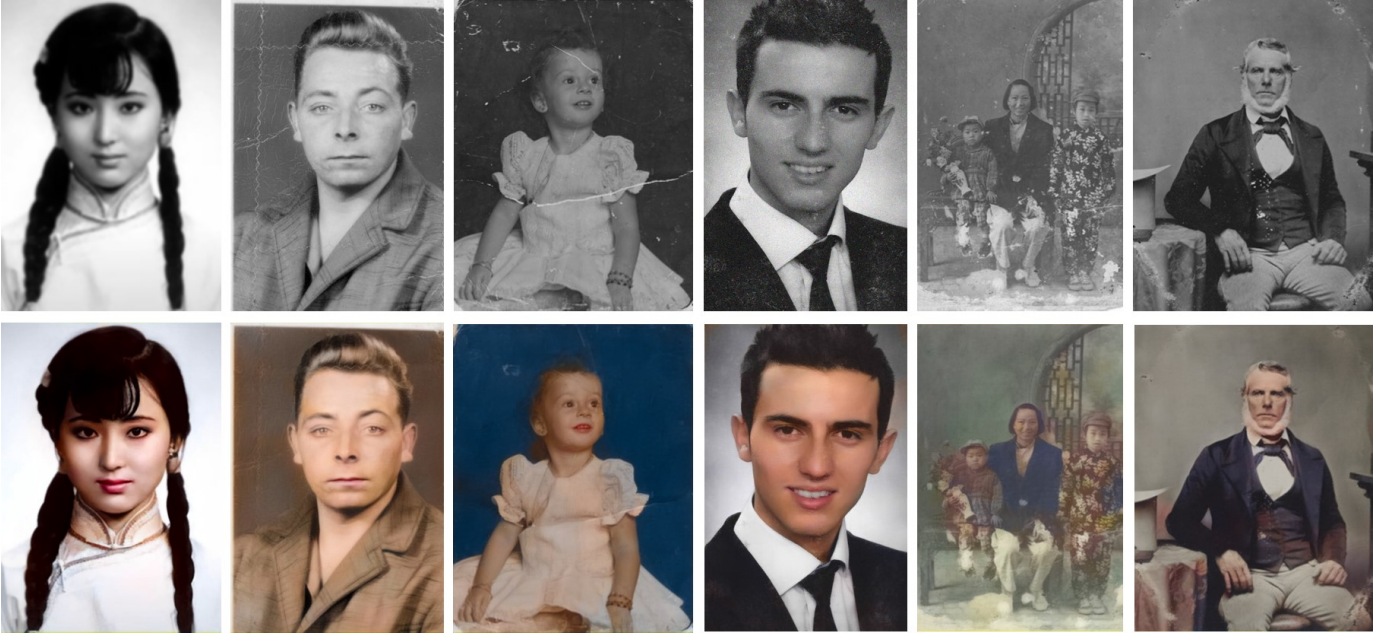


Fig. 1. Old photo renovation generated by the proposed ROMNet. The proposed framework is capable of simultaneously repairing multiple image degradations by joint restoration and colorization.

training data;

- A *reference-based multi-scale spatial-preserving color histogram fusion method for image colorization* is proposed to learn the content-aware transfer function between the input and reference signals;

- We construct the *first publicly available real-world old photo dataset* of 200 corrupted grayscale old photos for evaluation. Each of them is paired with a manually restored and colorized ‘pristine’ image by Adobe Photoshop experts;

- Our experimental results show that ROMNet achieves better visual and numerical performance over the state-of-the-art methods on both synthetic and our real-world datasets.

The rest of this paper is organized as follows. Section II reviews previous literature relevant to image colorization and old photo restoration, while Section III details our proposed ROMNet model. Experimental results and concluding remarks are given in Section IV and Section V, respectively.

## II. RELATED WORK

### A. Image Colorization

Image colorization aims at colorizing gray-scale images with natural colors. Before the emergence of deep neural networks, conventional methods for image colorization can be categorized into two streams, *i.e.*, *scribble-based* approaches and *example-based* methods. *Scribble-based* approaches [18]–[23] highly rely on user scribbles (*e.g.*, strokes) and guidance to colorize images. Colorization is generally formulated as a constrained optimization problem, which propagates user-defined color scribbles by similarity metrics. Although these methods can produce realistic colorized images with detailed guidance from the user, the process is very labor-intensive. *Example-based* methods have been developed, where color

statistics are extracted and used as references from user-specified images or Internet database to colorize the input gray-scale images [11]–[13], [24]–[27]. Although example-based methods reduce the labor cost, the colorization performance highly depends on the selected reference images. Several ways to compute the correspondences between the input images and the reference images are proposed, including pixel level [24], [26], semantic level [11], [25], and super-pixel level [12], [27] similarities.

Most recently, with the development of machine learning and deep learning, deep neural networks have shown promise in automatic image colorization [9], [28]–[34], where semantics and multi-modality are two identified critical points for successful colorization. [29] and [30] design two-branch architectures to explicitly learn and fuse the local image features and global semantic labels. [35] argues that pixel-level and image-level information is not sufficient for learning object appearance variations and further proposes to incorporate object-level information into its architecture. In terms of cross-modality, some works [9], [28], [30] replace single color prediction with per-pixel color distribution prediction, which yields more smooth visual effects.

### B. Image Restoration

Image degradation appears in various types, including noise, blurriness, color fading, low resolution, and crack. Traditional approaches to restore degraded image usually involve specified image prior constraints, such as non-local self-similarity [36], sparsity [37], local smoothness [38], etc. Most recently, deep learning-based methods have been dominating in many image restoration related tasks, such as image denoising [1], [39], [40], image super-resolution [3], [41], [42], and image deblurring [5], [43], [44], due to its capability of learning smooth semantic, perceptual and local image representations.

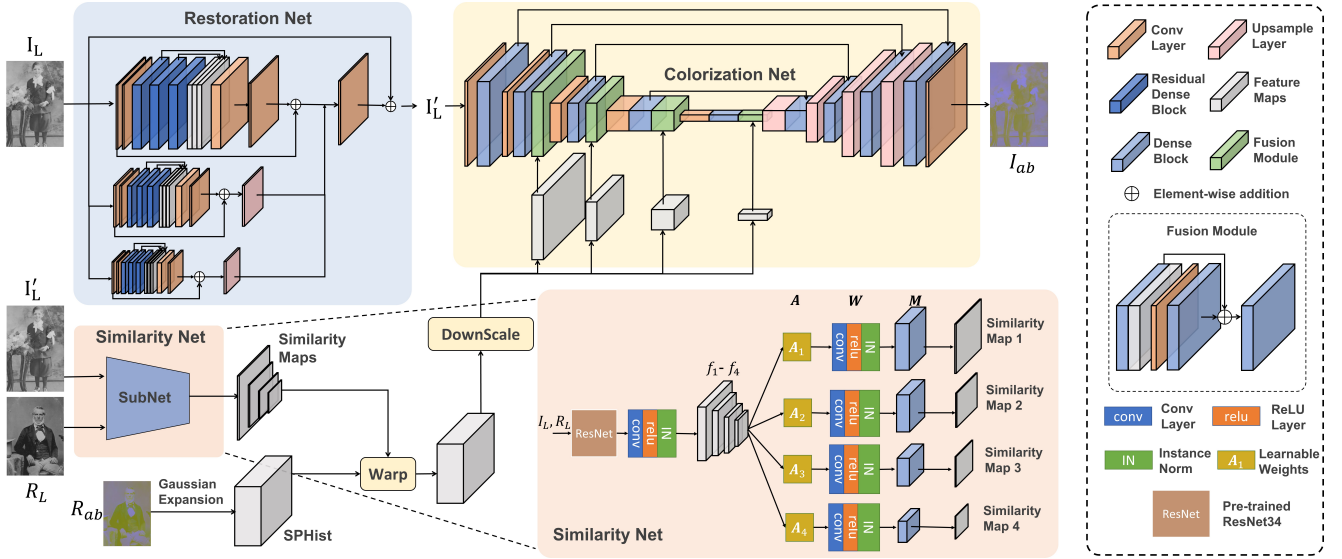


Fig. 2. System Pipeline.

To deal with the situation where various types of image degradation exist simultaneously under real-world settings, [45] designs a toolbox containing a series of operators, each of which takes care of one specific degradation. A learnable controller is proposed to select among the operators for image restoration. [46] proposes to employ an attention mechanism for automatic operator selection. [47] argues that deep neural networks can be used as an image prior for automatic image restoration without extra training data since deep neural networks resonate well with low-level image statistics.

### C. Old Photo Restoration.

Old Photo Restoration aims at restoring old photos with natural colors and formats. The identified challenges in this task include color restoration and degradation restoration. Most of the existing models only take care of one particular aspect of old photo restoration, e.g., color restoration or degradation restoration. However, renovating real-world old photos generally requires both colorization and restoration. [48] designs an image-level pixel-to-pixel image translation framework using paired synthetic and real images. Deoldify [49] also implements a pixel-to-pixel image translation and provides implementation in GAN settings. [47] learns single-degradation image restoration well in an unsupervised manner. [17] first encodes the data to latent representations, which separates old photo, ground truth, and synthetic image. Then, it learns image restoration while learning a latent translation.

Although previous attempts yield satisfying perceptual qualities by conducting colorization solely, old photo restoration requires both colorization and image quality restoration under real-world settings. Our work leverages both learning-based restoration and example-based color restoration methods for real-world old photo renovation. More importantly, since the example-based colorization technique is employed, our model uses much less training data.

## III. METHODOLOGY

There are two major challenges for old photo restoration and colorization. First, complicated degradation is generally observed in real-world old photos, which is hard to model and include in training data. Without first dealing with degradation, colorization results will be sub-optimal. Second, colorization is an ill-posed and ambiguous problem [50]. To achieve decent perceptual quality, most of the existing models demand a large-scale dataset such as ImageNet [10] for training, which is time-consuming and energy inefficient.

To overcome the challenges mentioned above, we propose an end-to-end trainable framework as Fig. 2 depicts. Specifically, after being converted into CIE Lab color space, each image is described by a lightness channel, i.e.,  $L$  and two chrominance channels, i.e.,  $a$  and  $b$ . Given a degraded gray-scale image  $I_L \in \mathbb{R}^{H \times W \times 1}$ , the restoration sub-net will first handle the degradation and produce a restored gray-scale image  $I'_L \in \mathbb{R}^{H \times W \times 1}$ . Then the  $I'_L$  and the lightness channel of the selected reference image  $R_L \in \mathbb{R}^{H \times W \times 1}$  are fed into the similarity sub-net jointly, obtaining the similarity map between them. After that, the extracted color features from the  $ab$  channels of the reference image  $R_{ab} \in \mathbb{R}^{H \times W \times 2}$  will be projected to the input image space. The colorization sub-net takes  $I'_L$  and the projected reference color feature together as inputs jointly to generate the  $ab$  channels of the input  $I_{ab} \in \mathbb{R}^{H \times W \times 2}$  and concatenate it with  $I'_L$  to get the final output  $I_{Lab} \in \mathbb{R}^{H \times W \times 3}$ .

Note that while previous works choose to directly feed the raw  $ab$  channels of the reference image [13], [14] or utilize the mean and variance of adaptive instance normalization layer of the reference image [16], [51], in this work, we come up with a multi-scale fusion method that combines both the spatial-preserve color histogram and deep learning-based features. The spatial-preserve color histogram offers strong prior knowledge of statistical color and spatial information, and they are aggregated at multiple scales to fully

exploit the prior knowledge to enable learning colorization within finite training samples. These multi-level color histogram features will concatenate with the intermediate deep features in the encoder and take advantage of convolutional filters to achieve a robust fusion. In such a way, the network is insensitive to the reference selection. The details of the restoration sub-net, similarity sub-net, colorization sub-net, and our reference selection algorithms will be elaborated in the following sections.

### A. Restoration Sub-Net

In general, the degradation in old photos can be divided into two categories: the structured defects (*e.g.*, cracks, smudges) and unstructured defects (*e.g.*, image blur, dust effect, film noises) [17]. The structure defects require a large receptive field for neural networks to capture global contexts to recover structural integrity. On the other hand, neural networks need to fully exploit local information to handle unstructured defects. In this work, we develop a multi-level Residual Dense Network (RDN [52]). RDN has demonstrated outstanding performance on common image restoration tasks such as image super-resolution, denoising, and deblurring, mainly facilitated by its core module called the residual dense block. The residual dense block is designed to fully extract abundant information via dense connection and contiguous memory mechanisms, and such architecture is suitable for eliminating the unstructured defects. However, RDN processes images on the same resolution, which restricts the size of receptive field of neural networks and weakens its capability to solve structured flaws. Thus, we extend the original RDN into a multi-level structure to enlarge the receptive field to better repair structured flaws.

As Fig. 2 depicts, the original input image and its 4× and 8× downsampled versions are fed into top, second, and third levels of RDN, respectively. Each level consists of three residual dense blocks, each of which is composed of 4 identical residual dense units. The outputs of the lower levels will be upsampled via bilinear interpolation and fused via concatenation, then go through another convolution layer to generate  $I'_L$ .

### B. Similarity Sub-Net

After the refined lightness map  $I'_L$  is obtained from the restoration sub-net, it will be passed to the similarity sub-net together with the selected reference image's lightness channel  $R_L$ . The similarity sub-net is designed to project the reference image features into the feature space of the input image. The architecture of the similarity sub-net is similar to the one used in [14], which takes advantage of the powerful convolutional neural network to manipulate robust dense matching. As illustrated in the Similarity Net in Fig. 2, a pre-trained ResNet34 [53] is employed to retrieve layer1, layer2, layer3, layer4 feature maps from the input and reference images. Note that these feature maps have progressively smaller spatial resolutions and more channels with as going deeper with the network. Then four different convolution filters will be applied to these intermediate features to get new feature maps that

have the same channels  $f_i \in \mathbb{R}^{H_i \times W_i \times C}$  ( $i = 1, 2, 3, 4$ ). Different from [14] using a single-scale similarity map, we utilize similarity maps at different scales for later multi-level feature fusion in the colorization net. Since simply resizing and concatenating these four feature maps as in [14] will regard each feature map contributing equally at a different level and ignore the scale information, we propose to construct a learnable coefficient  $A_i \in \mathbb{R}^{1 \times 4}$ , where  $i=1$  to 4, to assign different weights to the feature maps depending on the target similarity map size. These weighted feature maps will then be concatenated together to obtain a feature tensor. For instance, the concatenated feature  $M_i \in \mathbb{R}^{H_i \times W_i \times C}$  at scale  $i$  would be:

$$M_i = W \otimes [g(A_{i1} * f_1) \oplus g(A_{i2} * f_2) \oplus g(A_{i3} * f_3) \oplus g(A_{i4} * f_4)], \quad (1)$$

where  $W$  is the shared convolution filter for the convolution computation  $\otimes$ ,  $g$  represents up-sampling or down-sampling function to align the feature size to target similarity map size,  $*$  indicates the element-wise multiplication, and  $\oplus$  denotes concatenate operation. Subsequently, the three-dimensional feature  $M_i$  will be reshaped to two-dimension matrix  $\bar{M}_i \in \mathbb{R}^{H_i W_i \times C}$ . The similarity map characterizing the correlation between the reference  $R$  and the input  $I$  at scale level  $i$ ,  $\Phi_{R \leftrightarrow I}^i \in \mathbb{R}^{H_i W_i \times H_i W_i}$ , will be computed. The element of the similarity map at the the spatial location  $(u, v)$  can be calculated as follow:

$$\Phi_{R \leftrightarrow I}^i(u, v) = \frac{(\bar{M}_i^I(u) - \mu_{\bar{M}_i^I}) \cdot (\bar{M}_i^R(v) - \mu_{\bar{M}_i^R})}{\|\bar{M}_i^I(u) - \mu_{\bar{M}_i^I}\|_2 \|\bar{M}_i^R(v) - \mu_{\bar{M}_i^R}\|_2}, \quad (2)$$

where  $\mu_{\bar{M}_i^I}$  and  $\mu_{\bar{M}_i^R}$  are the mean feature vectors. The softmax function will then be applied to the similarity map along the x-axis, so each element is within  $[0, 1]$ . This similarity map will be used in the colorization sub-net to align the information of the reference image with the input image.

### C. Colorization Sub-Net

To tackle the aforementioned colorization problem, we propose to use Spatial-Preserve color Histogram (SPHist) from reference images for information fusion. Unlike the traditional color histogram, the proposed SPHist can keep the spatial information of the image and indicate the probability of each pixel falling in each bin. More importantly, *SPHist is differentiable*, and thus, it can be used in an end-to-end neural network using gradient back-propagation for training. In particular, we used Gaussian expansion [54] to approximate the SPHist of each channel separately  $h \in \mathbb{R}^{H \times W \times K}$ , where  $K$  is the number of bins. The probability of a pixel at location  $(i, j)$  falling into the  $k$ -th bin is calculated as follow:

$$h(i, j, k) = \frac{\exp(-\frac{(D_{ij}-u_k)^2}{2\sigma^2})}{\sum_{k=1}^K \exp(-\frac{(D_{ij}-u_k)^2}{2\sigma^2})}, \quad (3)$$

where  $D_{ij}$  is the pixel value of  $a$  or  $b$  channel of the reference image at location  $(i, j)$ ;  $\sigma$  is the standard deviation of Gaussian distribution that is set to 0.1 empirically in our setting;  $u_k$  is



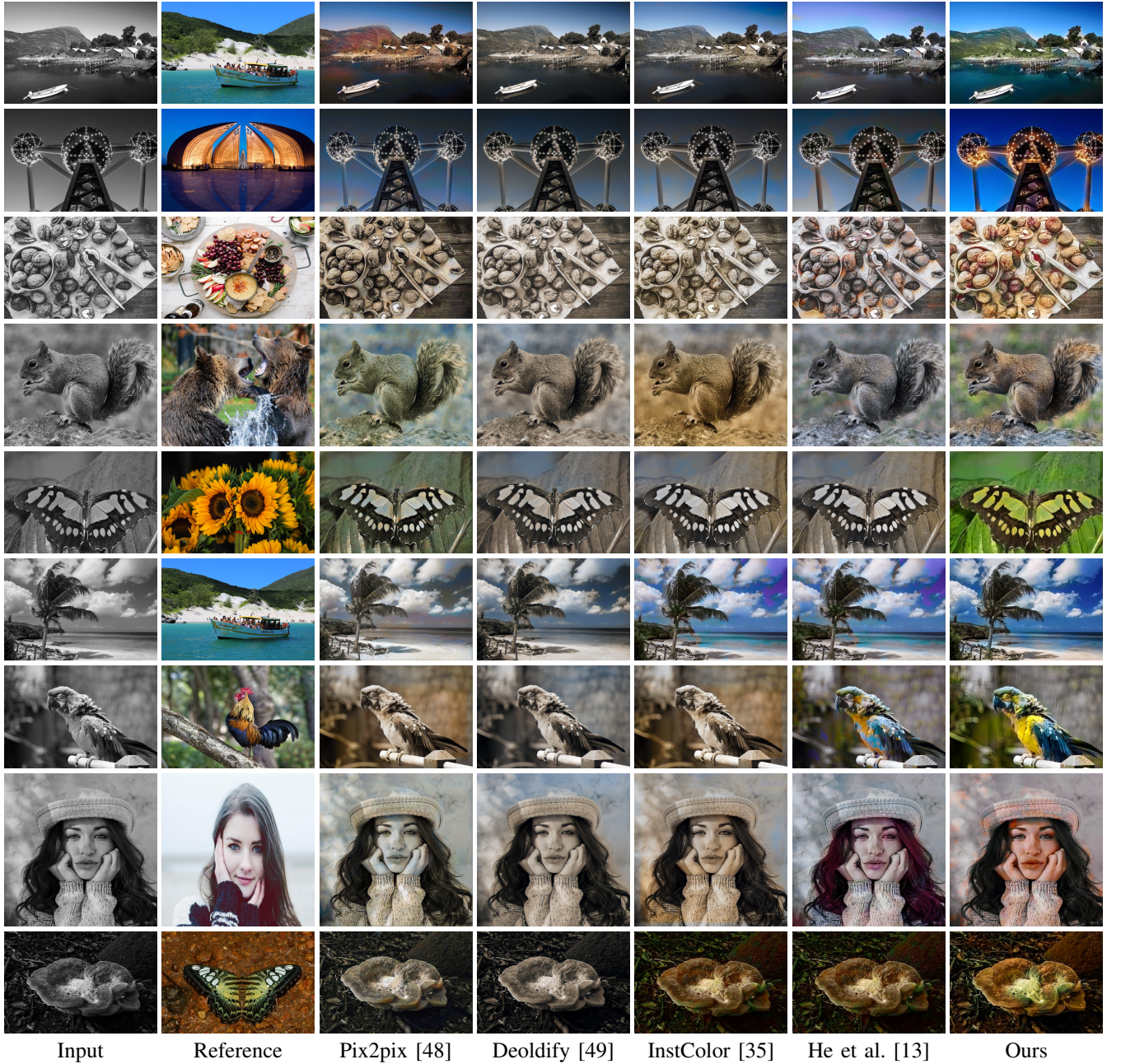


Fig. 3. Visual comparisons against state-of-the-art colorization methods on DIV2K. It shows that with only 800 training images, our method is able to accomplish visually pleasant colorization and our result is significantly better than others.

an learnable parameter representing the center of bin  $k$ , which is initialized as follow:

$$u_k^0 = v_{min} + \frac{v_{max} - v_{min}}{K} * k, \quad (4)$$

where  $v_{min}$  and  $v_{max}$  are the minimum and maximum value of  $ab$  channels, which are -1 and 1 respectively in our experiment. Although the bins are equally distributed at the beginning, after training for several iterations, the distribution will be unequal. We set this on purpose as some colors might be rarer than others in the wild. The extracted color histogram will be reshaped to  $\bar{h} \in \mathbb{R}^{HW \times K}$  and down-sampled to different scales to perform matrix multiplication with the corresponding-scale similarity maps, leading to a warped SPHist. The warped

SPHist contains the similarity-guided spatial-preserve color histogram information from the reference image. Then the warped SPHist will be fed into different levels of the encoder in the colorization sub-network for the color prediction.

The backbone is a modified version of U-Net [55], as it has demonstrated promising performance in many fields, such as medical image segmentation [56]–[59] and autonomous driving [60], [61]. Here we replace the convolutional layers in U-Net with densely connected modules [62]. There are four dense blocks in the encoder containing 6, 12, 24, and 16 dense units. The decoder shares a similar structure with the encoder, and bi-linear interpolation is employed to upscale the forwarding features between dense blocks. The warped SPHist

extracted from the reference image will be concatenated with the intermediate features after each dense block in the encoder as the input of the fusion module. The fusion module contains a dense block with six dense units and a  $3 \times 3$  convolution layer, which is responsible for combining the traditional color heuristics and deep features efficiently to enable efficient colorization. Since the information of reference is fused in the intermediate levels instead of at the beginning, the model will learn how to deal with the dissimilarity between input and reference image. Also, multi-level fusion well aggregates the reference information.

#### D. Training Objective

In order to 1) simultaneously train the restoration and colorization nets, 2) exploit the rich color information in the reference image, and 3) improve the visual quality of the overall restored output, we employed a weighted sum of various objectives such that the whole system can be trained end-to-end. Among these, *luminance reconstruction loss* between the restored luminance  $I'_L$  and the ground truth luminance  $G_L$  is adopted to supervise the training of restoration subnet:

$$\mathcal{L}_{rec,L} = \|I'_L - G_L\|_1. \quad (5)$$

However, it was generally observed that only using  $\ell_p$  norms as loss function tends to generate blurred estimates for image restoration [3]. Hence, we also used the *perceptual loss*, which has been shown to deliver better visual quality in multiple restoration tasks [3], [63], [64]. The relu22, relu32, relu42, and relu52 layers of VGG19 [65] are adopted:

$$\mathcal{L}_{perc,L} = \sum_j \frac{1}{C_j H_j W_j} \|\phi_j(I'_L) - \phi_j(G_L)\|_2^2, \quad (6)$$

where  $\phi_j$  is a feature map of shape  $C_j \times H_j \times W_j$ .

The colorization subnet is expected to transfer the color distributions from the reference image to the predicted output. *Histogram loss* is leveraged to measure the distribution loss between the color histograms of output and reference signals by measuring their Earth Mover's Distance (EMD):

$$\mathcal{L}_{EMD,h} = \sum_{k=1}^K (\text{CDF}_{h_{I'}}(k) - \text{CDF}_{h_R}(k))^2, \quad (7)$$

where  $\text{CDF}_p(k)$  is the  $k$ -th element of the cumulative density function of probability mass function  $p$ .  $h_{I'}$  and  $h_R$  are one-dimensional differentiable histograms which is the global sum pooling result of the SPHists  $h_{I'}$  and  $h_R$  mentioned in Eq. (3), respectively.

We also applied *chroma reconstruction loss* to impose the spatial consistency between the predicted  $ab$  and ground truth  $ab$  channels to supplement the histogram loss:

$$\mathcal{L}_{rec,ab} = \|I'_{ab} - G_{ab}\|_1. \quad (8)$$

The *adversarial loss* is a common recipe to enhance the visual quality of synthesized images [3], [66], [67]. Here we adopted PatchGAN [34] structure to ensure all local patches of

enhanced output channels visually similar to realistic chroma maps. The adversarial loss is expressed as:

$$\mathcal{L}_{adv,ab} = \mathbb{E}_{G_{ab}}[\log D(G)] + \mathbb{E}_{I'_{ab}}[\log(1 - D(I', R))]. \quad (9)$$

Finally, the overall objective/loss function for training ROMNet is thus written as:

$$\mathcal{L} = \alpha \mathcal{L}_{rec,L} + \beta \mathcal{L}_{perc,L} + \lambda \mathcal{L}_{EMD,h} + \gamma \mathcal{L}_{rec,ab} + \eta \mathcal{L}_{adv,ab}. \quad (10)$$

#### E. Reference Selection

As discussed earlier, our proposed ROMNet requires a reference color image as an additional input to guide the colorization process. Thus, we propose an automatic reference selection scheme that is able to generate good references from a database, given an input grayscale image, for both training and inference phases.

An ideal reference is expected to be both visually and semantically similar to the target image, meanwhile providing rich color information for target colorization. Inspired by the widely used deep features for perceptual similarity modeling [68], [69], we leveraged a pre-trained image classification network VGG19 [65] as the backbone to extract intermediate deep feature maps. Then, we define the texture and the structural similarity between one grayscale input image and one color image using the global mean and variance/covariance of feature maps, respectively [69]. The weighted summation of the texture and structure similarity is used to discover the reference color image in the training set with top similarity to the grayscale input image. When used for prediction, the users can either choose a recommended reference retrieved from an image corpus, or manually select one, depending on their preference.

## IV. EXPERIMENTS

#### A. Experimental setting

**Dataset** We train and evaluate our method on three datasets: *Div2K* [70]: Div2K was first introduced for image super-resolution, which contains 1,000 RGB high-resolution images being split into a training set (800 images), a validation set (100 images), and a testing set (100 images). Note that this dataset is only used to illustrate the effectiveness of the proposed colorization sub-net on performing colorization for images with complex scenarios and limited training data. In our experiment, we employed the training and validation sets for model training and testing, respectively. Moreover, to show that our model has a loose constraint on the selection of references, during inference, references for testing images in the validation set can only be drawn from the training set, which contains only 800 images, instead of from ImageNet, which provides millions of choices.

*Pascal* [71]: In order to produce realistic defects, similar with [17], we gather crack and dust-paper textures and hire Photoshop experts to extract the degradation patterns from some real old photos that are not in our proposed RealOld dataset, and blend the textures and extracted degradation patterns with images in Pascal dataset using alpha compositing





Fig. 4. Visual comparisons against state-of-the-art colorization and restoration methods on RealOld dataset. It shows that with the limited synthetic training data from Pascal, our model is able to fix most of the degradation and deliver plausible colorization.



TABLE I  
QUANTITATIVE COMPARISON ON THE DIV2K AND PASCAL VOC VALIDATION DATASETS. UP-WARD ARROWS INDICATE THAT A HIGHER SCORE DENOTES A GOOD IMAGE QUALITY. WE HIGHLIGHT THE BEST SCORE FOR EACH MEASURE.

Dataset	DIV2K (w/o degradation)			Pascal VOC (w/o degradation)			Pascal VOC (w/ degradation)		
Metric	PSNR $\uparrow$	SSIM $\uparrow$	LPIPS $\downarrow$	PSNR $\uparrow$	SSIM $\uparrow$	LPIPS $\downarrow$	PSNR $\uparrow$	SSIM $\uparrow$	LPIPS $\downarrow$
Pix2pix	21.12	0.872	0.138	20.89	0.782	0.200	20.37	0.732	0.231
DeOldify	23.65	0.913	0.128	23.96	0.873	0.117	21.45	0.789	0.192
He <i>et al.</i>	23.53	0.918	0.125	23.85	0.925	0.114	-	-	-
InstColorization	22.45	0.914	0.131	23.95	0.932	0.111	-	-	-
Wan <i>et al.</i> -	-	-	-	-	-	-	18.01	0.598	0.421
Ours	<b>23.95</b>	<b>0.925</b>	<b>0.120</b>	<b>24.01</b>	<b>0.940</b>	<b>0.100</b>	<b>22.22</b>	<b>0.828</b>	<b>0.186</b>

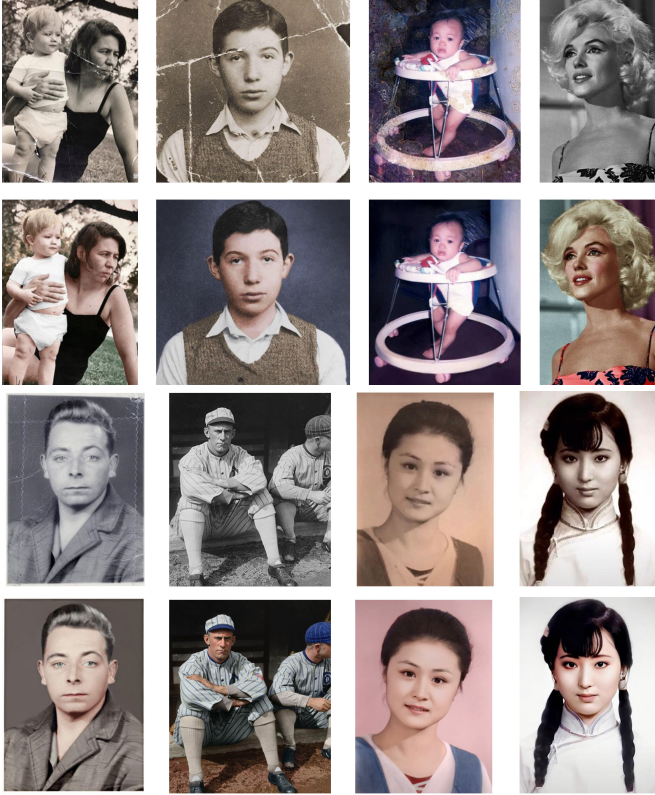


Fig. 5. Exemplary authentic old photos with their corresponding reference repaired by Photoshop expert sampled from our proposed RealOld test dataset.

with erratic transparency level to generate synthetic old photos. Furthermore, we add Gaussian blur and simulate severe photo damage by randomly setting a polygon area in the image to pure white. We select 10,000 images in Pascal as our training data and another 1,000 images as the testing set. Same as for Div2K dataset, the reference images for inference are retrieved from the training set. For Pascal, two different experiments are conducted: image restoration and colorization, and image colorization solely.

*Real-world Paired Old Photos (RealOld):* To validate the efficacy and generalizability of our model under real-world setting, we collect 200 real old black&white pictures paired with manually restored and colorized photos by Photoshop experts. To the best of our knowledge, this is the first real-world old photo dataset that has aligned “ground truth” to enable pixel-to-pixel evaluation. The constructed dataset contains

200 portraits with various backgrounds. Fig. 5 shows some sample image pairs from our proposed RealOld dataset. We hope this dataset opens a door to a new exciting journey, where in addition to colorization, distinct categories of degradation, including scratches, damages, dust effects, wornness, film noise, and loss of resolution existed in old photos, should also be dealt with. In our experiment, the RealOld is only used for testing after a model trained on Pascal. Furthermore, we randomly download 2,000 RGB portraits from Google images and utilize our algorithm to pick the best reference when testing the images of RealOld.

**Evaluation Metrics.** We report the peak signal-to-noise ratio (PSNR) and the structural similarity index (SSIM) [72] to compare the low-level differences between model outputs and ground truths. Learned perceptual image patch similarity (LPIPS) [73] is also employed, which has been shown better correlated with human perception.

**Training Details.** ROMNet is trained in an end-to-end manner using the Adam solver [74] with  $\beta_1 = 0.99, \beta_2 = 0.999$ . The initial learning rate is 0.0001 and will be decreased exponentially at the end of each epoch with a decay rate of 0.99. The loss balance weights are set empirically as follows:  $\alpha = 1.0, \beta = 0.2, \lambda = 0.5, \gamma = 1.0, \eta = 0.2$ . During training, for data augmentation purposes, patches with a resolution of  $256 \times 256$  are randomly cropped from the input images as input. For each epoch, we select one of the following two options for reference image generation: 1) a patch is cropped from the corresponding RGB image at a location different from that of the patch used as input, and processed with color jittering and affine transformation to create the reference; 2) ten images are firstly selected from the training set excluding the ground-truth image, from which, one picture is randomly selected as the reference. The models on DIV2K and Pascal are trained for 20 epochs, where each epoch takes about 1.5 minutes and 16 minutes, respectively, on a single GTX 3090Ti GPU.

## B. Experimental Results

Since no existing work explicitly considers image degradation and colorization simultaneously, we choose to compare our method with approaches in image-to-image translation (denoted as Pix2pix [75]), image restoration (denoted as Wan *et al.* [17]), and colorization (denoted as Deoldify [49], He *et al.* [13] and InstColorization [35]). For a fair comparison, we



TABLE II  
QUANTITATIVE COMPARISON ON THE REALOLD DATASET.

Dataset	Real old photo		
	PSNR $\uparrow$	SSIM $\uparrow$	LPIPS $\downarrow$
Pix2pix	16.80	0.684	0.320
DeOldify	17.14	0.723	0.287
He <i>et al.</i>	16.72	0.707	0.314
InstColorization	16.86	0.715	0.312
Wan <i>et al.</i>	16.99	0.709	0.303
<b>Ours</b>	<b>17.20</b>	<b>0.758</b>	<b>0.258</b>

TABLE III  
USER STUDY RESULTS ON THE REALOLD DATASET. THE PERCENTAGE % OF USER SELECTION IS SHOWN.

Method	Top 1	Top 2	Top 3	Top 4	Top 5
Pix2Pix [75]	3.1	11.8	24.3	41.6	67.7
Deoldify [49]	10.5	33.9	56.5	79.3	92.8
He <i>et al.</i> [13]	4.6	26.3	44.1	61.9	83.2
InstColorization [35]	8.0	26.3	53.6	75.5	92.2
Wan <i>et al.</i> [17]	23.1	38.6	48.9	59.1	72.0
<b>Ours</b>	<b>50.6</b>	<b>65.9</b>	<b>75.3</b>	<b>85.1</b>	<b>94.4</b>

will not evaluate InstColorization and He *et al.*, which could not restore degradation, on Pascal VOC with degradation; also, we will not compare with Wan *et al.*, which could not perform colorization, on the DIV2K without degradation and Pascal VOC without degradation. All the methods in comparison are trained from scratch using the training strategies and codes provided by authors.

1) *Quantitative Comparison*: Table I gives the quantitative results of the proposed model as well as the methods in comparison in two public datasets with three settings, *i.e.*, DIV2K without degradation, Pascal VOC without degradation, and Pascal VOC with degradation. Our proposed model yields the best scores in terms of all three evaluation metrics compared with the state-of-the-art methods. For example, in DIV2K dataset without degradation, our model achieves much better scores, *i.e.*, 23.95 (PSNR), 0.925 (SSIM), and 0.120 (LPIPS), compared with those produced by the comparison methods.

Table II shows the results on the RealOld dataset, where our model generates the best scores among the approaches in comparison, indicating the proposed method is the most resilient and suffers the least performance drop while transferring from the synthetic old photo datasets to the real old photo datasets.

2) *Qualitative Comparison*: Figure 3 presents the qualitative comparison on the DIV2K dataset, where the proposed method can yield results with vivid color while the results of the methods in comparison suffer from incomplete colorization. Fig. 4 shows the results on the RealOld dataset, where our approach can jointly perform image restoration and colorization, producing perceptually satisfying results.

3) *User Study*: We conduct a user study to compare all the methods to further demonstrate the effectiveness of the proposed method. We randomly choose 100 old photos from the RealOld dataset, and let users rank the results based on their subjective visual perception. We gathered reports from 15 people and presented the result in Table III. Our method

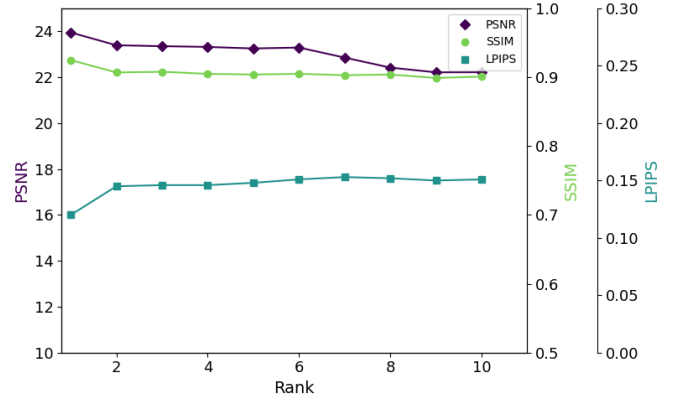


Fig. 6. Sensitivity analysis of reference image selection.

TABLE IV  
ABLATION STUDY OF MULTI-SCALE SPHIST ON DIV2K.

Method	PSNR $\uparrow$	SSIM $\uparrow$	LPIPS $\downarrow$
Input <i>ab</i> fusion	22.978	0.902	0.130
Multi-scale <i>ab</i> fusion	23.233	0.910	0.127
Single-scale histogram fusion	23.631	0.906	0.125
Multi-scale histogram fusion	<b>23.952</b>	<b>0.925</b>	<b>0.120</b>

has a high probability of 50.6% to be selected as the top-1 rank and outperforms other methods over all rankings, which further illustrates the superiority of our ROMNet in terms of image restoration and colorization.

### C. Ablation Study

**Multi-scale SPHist.** We conduct three experiments on the Div2k dataset to evaluate the effectiveness of our multi-scale SPHist: 1) following [13], the transferred *ab* channels of the reference and the *L* channel of the input are directly concatenated and fed into the backbone of our colorization sub-net; 2) instead of using the multi-scale SPHist of the reference image, we employ the multi-scale raw *ab* channels of the reference image as input; 3) we only fuse a single-scale color histogram with the encoder in the shallower layer. The results are reported in Table IV, which validates the importance and usefulness of our multi-scale SPHist.

**Multi-scale Similarity Maps.** To validate the superior of the multi-scale similarity maps design over single similarity map, we further conduct two experiments: 1) we use the origin single-scale similarity map proposed by [14]; 2) no similarity map is applied to the reference image. Table V reflects the benefits brought by the multi-scale similarity maps.

**Multi-scale RDN.** In order to prove the performance gain brought by the multi-level Residual Dense Network (RDN [52]), we also select the origin RDN as the backbone for old photo restoration and test on the Pascal [71] dataset with degradation. The results in Table VI demonstrates that the multi-level design can effectively improve the restored outputs.

**Sensitivity to Reference Image Selection.** To confirm the robustness of our model to the reference image selection, we compare the results on the DIV2K dataset using the different reference images from the most similar one (rank 1) to the

TABLE V  
ABLATION STUDY OF MULTI-SCALE SIMILARITY MAPS ON DIV2K.

Method	PSNR $\uparrow$	SSIM $\uparrow$	LPIPS $\downarrow$
No similarity map	22.817	0.910	0.131
Single-scale similarity map	23.803	0.922	0.126
Multi-scale similarity map	<b>23.952</b>	<b>0.925</b>	<b>0.120</b>

TABLE VI  
ABLATION STUDY OF MULTI-LEVEL RDN ON PASCAL WITHO  
DEGRADATION.

Method	PSNR $\uparrow$	SSIM $\uparrow$	LPIPS $\downarrow$
Single-level RDN	21.89	0.818	0.190
Multi-level RDN	<b>22.22</b>	<b>0.828</b>	<b>0.186</b>

least similar one (rank 10) among the ten selected reference images. As Fig. 6 depicts, the performance of our model is robust with only slight drops, *i.e.*, from 23.95 (rank 1) to 22.25 (rank 10) for PSNR, from 0.925 (rank 1) to 0.899 (rank 10) for SSIM, and from 0.12 (rank 1) to 0.15 (rank 10) for LPIPS.

## V. CONCLUSION

We propose *the first end-to-end trainable network* (named ROMNet) to restore mixed degradations in old photos by joint restoration and colorization with a color reference. The whole system contains several submodules, each of which is designed to handle a single defect. Specifically, a hierarchical restoration subnet is applied to recover the scratches and damages in the luminance channel, followed by a colorization U-Net that leverages the spatial-preserve color histograms of the reference image to estimate the chroma components, conditioned on the luminance similarity. Our method learns more efficiently with limited training data, owing to a hybrid of learning- and example-based structure and the use of a similarity net that aligns the reference signal with the input. Extensive experimental results demonstrated that ROMNet attains promising performance both visually and numerically on synthetic and real old photo datasets compared with the state-of-the-arts. Moreover, we also created *the first publicly available real-world old photo dataset* that includes 200 pairs of authentic legacy photographs with corresponding “ground truth” repaired by Photoshop experts, which we believe will facilitate further research on deep learning-based old photo restoration and enhancement.

## REFERENCES

- [1] K. Zhang, W. Zuo, and L. Zhang, “Ffdnet: Toward a fast and flexible solution for cnn-based image denoising,” *IEEE Trans. Image Process.*, vol. 27, no. 9, pp. 4608–4622, 2018.
- [2] Z. Meng, R. Xu, and C. M. Ho, “Gin-net: Global information aware network for low-light imaging,” in *European Conference on Computer Vision*. Springer, 2020, pp. 327–342.
- [3] C. Ledig, L. Theis, F. Huszar, J. Caballero, A. Cunningham, A. Acosta, A. Aitken, R. Xu, and C. M. Ho, “Photo-realistic single image super-resolution using a generative adversarial network,” in *Proc. IEEE Conf. Comput. Vis. Pattern Recognit. (CVPR)*, 2017, pp. 4681–4690.
- [4] Y. Mei, Y. Zhao, and W. Liang, “Dsr: An accurate single image super resolution approach for various degradations,” in *2020 IEEE International Conference on Multimedia and Expo (ICME)*. IEEE, 2020, pp. 1–6.

- [5] S. Nah, T. Hyun Kim, and K. Mu Lee, “Deep multi-scale convolutional neural network for dynamic scene deblurring,” in *Proc. IEEE Conf. Comput. Vis. Pattern Recognit. (CVPR)*, 2017, pp. 3883–3891.
- [6] Z. Tu, H. Talebi, H. Zhang, F. Yang, P. Milanfar, A. Bovik, and Y. Li, “Maxim: Multi-axis mlp for image processing,” *arXiv preprint arXiv:2201.02973*, 2022.
- [7] J. Ballé, V. Laparra, and E. P. Simoncelli, “End-to-end optimized image compression,” *arXiv preprint arXiv:1611.01704*, 2016.
- [8] L.-H. Chen, C. G. Bampis, Z. Li, A. Norkin, and A. C. Bovik, “Proxiqa: A proxy approach to perceptual optimization of learned image compression,” *IEEE Transactions on Image Processing*, vol. 30, pp. 360–373, 2020.
- [9] R. Zhang, P. Isola, and A. A. Efros, “Colorful image colorization,” in *Proc. Eur. Conf. Comput. Vis. (ECCV)*. Springer, 2016, pp. 649–666.
- [10] J. Deng, W. Dong, R. Socher, L.-J. Li, K. Li, and L. Fei-Fei, “Imagenet: A large-scale hierarchical image database,” in *Proc. IEEE Conf. Comput. Vis. Pattern Recognit. (CVPR)*. Ieee, 2009, pp. 248–255.
- [11] R. Ironi, D. Cohen-Or, and D. Lischinski, “Colorization by example,” in *Rendering Techniques*. Citeseer, 2005, pp. 201–210.
- [12] R. K. Gupta, A. Y.-S. Chia, D. Rajan, E. S. Ng, and H. Zhiyong, “Image colorization using similar images,” in *Proc. ACM Multimedia Conf. (MM)*, 2012, pp. 369–378.
- [13] M. He, D. Chen, J. Liao, P. V. Sander, and L. Yuan, “Deep exemplar-based colorization,” *ACM Trans. Graphics*, vol. 37, no. 4, pp. 1–16, 2018.
- [14] B. Zhang, M. He, J. Liao, P. V. Sander, L. Yuan, A. Bermak, and D. Chen, “Deep exemplar-based video colorization,” in *Proc. IEEE Conf. Comput. Vis. Pattern Recognit. (CVPR)*, 2019, pp. 8052–8061.
- [15] R. Zhang, “Image synthesis for self-supervised visual representation learning,” Ph.D. dissertation, UC Berkeley, 2018.
- [16] S. Yoo, H. Bahng, S. Chung, J. Lee, J. Chang, and J. Choo, “Coloring with limited data: Few-shot colorization via memory-augmented networks,” in *Proc. IEEE Conf. Comput. Vis. Pattern Recognit. (CVPR)*, June 2019.
- [17] Z. Wan, B. Zhang, D. Chen, P. Zhang, D. Chen, J. Liao, and F. Wen, “Bringing old photos back to life,” in *Proc. IEEE Conf. Comput. Vis. Pattern Recognit. (CVPR)*, 2020, pp. 2747–2757.
- [18] A. Levin, D. Lischinski, and Y. Weiss, “Colorization using optimization,” in *ACM SIGGRAPH*, 2004, pp. 689–694.
- [19] Y.-C. Huang, Y.-S. Tung, J.-C. Chen, S.-W. Wang, and J.-L. Wu, “An adaptive edge detection based colorization algorithm and its applications,” in *Proc. ACM Multimedia Conf. (MM)*, 2005, pp. 351–354.
- [20] L. Yatziv and G. Sapiro, “Fast image and video colorization using chrominance blending,” *IEEE Trans. Image Process.*, vol. 15, no. 5, pp. 1120–1129, 2006.
- [21] Y. Qu, T.-T. Wong, and P.-A. Heng, “Manga colorization,” *ACM Trans. Graphics*, vol. 25, no. 3, pp. 1214–1220, 2006.
- [22] Q. Luan, F. Wen, D. Cohen-Or, L. Liang, Y.-Q. Xu, and H.-Y. Shum, “Natural image colorization,” in *Eurographics Conf. Render. Technol.*, 2007, pp. 309–320.
- [23] D. Šykora, J. Dingliana, and S. Collins, “Lazybrush: Flexible painting tool for hand-drawn cartoons,” in *Comput. Graphics Forum*, vol. 28, no. 2. Wiley Online Library, 2009, pp. 599–608.
- [24] T. Welsh, M. Ashikhmin, and K. Mueller, “Transferring color to greyscale images,” in *Annual Conf. Comput. Graphics Interactive Techniques*, 2002, pp. 277–280.
- [25] G. Charpiat, M. Hofmann, and B. Schölkopf, “Automatic image colorization via multimodal predictions,” in *Proc. Eur. Conf. Comput. Vis. (ECCV)*. Springer, 2008, pp. 126–139.
- [26] X. Liu, L. Wan, Y. Qu, T.-T. Wong, S. Lin, C.-S. Leung, and P.-A. Heng, “Intrinsic colorization,” in *ACM SIGGRAPH Asia*, 2008, pp. 1–9.
- [27] A. Y.-S. Chia, S. Zhuo, R. K. Gupta, Y.-W. Tai, S.-Y. Cho, P. Tan, and S. Lin, “Semantic colorization with internet images,” *ACM Trans. Graphics*, vol. 30, no. 6, pp. 1–8, 2011.
- [28] G. Larsson, M. Maire, and G. Shakhnarovich, “Learning representations for automatic colorization,” in *European Conference on Computer Vision*. Springer, 2016, pp. 577–593.
- [29] S. Iizuka, E. Simo-Serra, and H. Ishikawa, “Let there be color! joint end-to-end learning of global and local image priors for automatic image colorization with simultaneous classification,” *ACM Trans. Graphics*, vol. 35, no. 4, pp. 1–11, 2016.
- [30] J. Zhao, L. Liu, C. G. Snoek, J. Han, and L. Shao, “Pixel-level semantics guided image colorization,” *arXiv preprint arXiv:1808.01597*, 2018.
- [31] A. Deshpande, J. Rock, and D. Forsyth, “Learning large-scale automatic image colorization,” in *Proc. IEEE Int. Conf. Comput. Vis. (ICCV)*, 2015, pp. 567–575.

- [32] Z. Cheng, Q. Yang, and B. Sheng, "Deep colorization," in *Proc. IEEE Int. Conf. Comput. Vis. (ICCV)*, 2015, pp. 415–423.
- [33] R. Zhang, J.-Y. Zhu, P. Isola, X. Geng, A. S. Lin, T. Yu, and A. A. Efros, "Real-time user-guided image colorization with learned deep priors," *arXiv preprint arXiv:1705.02999*, 2017.
- [34] P. Isola, J.-Y. Zhu, T. Zhou, and A. A. Efros, "Image-to-image translation with conditional adversarial networks," in *Proc. IEEE Conf. Comput. Vis. Pattern Recognit. (CVPR)*, 2017, pp. 1125–1134.
- [35] J.-W. Su, H.-K. Chu, and J.-B. Huang, "Instance-aware image colorization," in *Proc. IEEE Conf. Comput. Vis. Pattern Recognit. (CVPR)*, 2020, pp. 7968–7977.
- [36] A. Buades, B. Coll, and J.-M. Morel, "A non-local algorithm for image denoising," in *Proc. IEEE Conf. Comput. Vis. Pattern Recognit. (CVPR)*, vol. 2, IEEE, 2005, pp. 60–65.
- [37] M. Elad and M. Aharon, "Image denoising via sparse and redundant representations over learned dictionaries," *IEEE Trans. Image process.*, vol. 15, no. 12, pp. 3736–3745, 2006.
- [38] Y. Weiss and W. T. Freeman, "What makes a good model of natural images?" in *Proc. IEEE Conf. Comput. Vis. Pattern Recognit. (CVPR)*, IEEE, 2007, pp. 1–8.
- [39] K. Zhang, W. Zuo, S. Gu, and L. Zhang, "Learning deep cnn denoiser prior for image restoration," in *Proc. IEEE Conf. Comput. Vis. Pattern Recognit. (CVPR)*, 2017, pp. 3929–3938.
- [40] K. Zhang, W. Zuo, Y. Chen, D. Meng, and L. Zhang, "Beyond a gaussian denoiser: Residual learning of deep cnn for image denoising," *IEEE Trans. Image Process.*, vol. 26, no. 7, pp. 3142–3155, 2017.
- [41] C. Dong, C. C. Loy, K. He, and X. Tang, "Learning a deep convolutional network for image super-resolution," in *Proc. Eur. Conf. Comput. Vis. (ECCV)*, Springer, 2014, pp. 184–199.
- [42] J. Kim, J. K. Lee, and K. M. Lee, "Accurate image super-resolution using very deep convolutional networks," in *Proc. IEEE Conf. Comput. Vis. Pattern Recognit. (CVPR)*, 2016, pp. 1646–1654.
- [43] L. Xu, J. S. Ren, C. Liu, and J. Jia, "Deep convolutional neural network for image deconvolution," *Adv. Neural Information Process. Syst.*, vol. 27, pp. 1790–1798, 2014.
- [44] J. Sun, W. Cao, Z. Xu, and J. Ponce, "Learning a convolutional neural network for non-uniform motion blur removal," in *Proc. IEEE Conf. Comput. Vis. Pattern Recognit. (CVPR)*, 2015, pp. 769–777.
- [45] K. Yu, C. Dong, L. Lin, and C. C. Loy, "Crafting a toolchain for image restoration by deep reinforcement learning," in *Proc. IEEE Conf. Comput. Vis. Pattern Recognit. (CVPR)*, 2018, pp. 2443–2452.
- [46] M. Suganuma, X. Liu, and T. Okatani, "Attention-based adaptive selection of operations for image restoration in the presence of unknown combined distortions," in *Proc. IEEE Conf. Comput. Vis. Pattern Recognit. (CVPR)*, 2019, pp. 9039–9048.
- [47] D. Ulyanov, A. Vedaldi, and V. Lempitsky, "Deep image prior," in *Proc. IEEE Conf. Comput. Vis. Pattern Recognit. (CVPR)*, 2018, pp. 9446–9454.
- [48] T.-C. Wang, M.-Y. Liu, J.-Y. Zhu, A. Tao, J. Kautz, and B. Catanzaro, "High-resolution image synthesis and semantic manipulation with conditional gans," in *Proc. IEEE Conf. Comput. Vis. Pattern Recognit. (CVPR)*, 2018, pp. 8798–8807.
- [49] J. Antic, "jantic/deoldify: A deep learning based project for colorizing and restoring old images (and video!)." [Online]. Available: <https://github.com/jantic/DeOldify>
- [50] G. Charpiat, M. Hofmann, and B. Schölkopf, "Automatic image colorization via multimodal predictions," vol. 2008, 09 2008.
- [51] Z. Xu, T. Wang, F. Fang, Y. Sheng, and G. Zhang, "Stylization-based architecture for fast deep exemplar colorization," in *Proc. IEEE Conf. Comput. Vis. Pattern Recognit. (CVPR)*, June 2020.
- [52] Y. Zhang, Y. Tian, Y. Kong, B. Zhong, and Y. Fu, "Residual dense network for image restoration," *IEEE Trans. Pattern Anal. Mach. Intell.*, vol. PP, pp. 1–1, 01 2020.
- [53] K. He, X. Zhang, S. Ren, and J. Sun, "Deep residual learning for image recognition," in *Proc. IEEE Conf. Comput. Vis. Pattern Recognit. (CVPR)*, 2016, pp. 770–778.
- [54] K. Schütt, F. Arbabzadah, S. Chmiela, K.-R. Müller, and A. Tkatchenko, "Quantum-chemical insights from deep tensor neural networks," *Nature Communications*, vol. 8, 01 2017.
- [55] O. Ronneberger, P. Fischer, and T. Brox, "U-net: Convolutional networks for biomedical image segmentation," in *Int. Conf. Medical Image Comput. Computer-assisted Intervention*. Springer, 2015, pp. 234–241.
- [56] H. Huang, L. Lin, R. Tong, H. Hu, Q. Zhang, Y. Iwamoto, X. Han, Y.-W. Chen, and J. Wu, "Unet 3+: A full-scale connected unet for medical image segmentation," in *ICASSP 2020-2020 IEEE International Conference on Acoustics, Speech and Signal Processing (ICASSP)*. IEEE, 2020, pp. 1055–1059.
- [57] Y. Du, Q. Quan, H. Han, and S. K. Zhou, "Where is the disease? semi-supervised pseudo-normality synthesis from an abnormal image," *arXiv preprint arXiv:2106.15345*, 2021.
- [58] Q. Quan, Q. Wang, L. Li, Y. Du, and S. K. Zhou, "Ct film recovery via disentangling geometric deformation and illumination variation: Simulated datasets and deep models," *arXiv preprint arXiv:2012.09491*, 2020.
- [59] P. Liu, H. Han, Y. Du, H. Zhu, Y. Li, F. Gu, H. Xiao, J. Li, C. Zhao, L. Xiao *et al.*, "Deep learning to segment pelvic bones: large-scale ct datasets and baseline models," *International Journal of Computer Assisted Radiology and Surgery*, vol. 16, no. 5, pp. 749–756, 2021.
- [60] R. Xu, F. Tafazzoli, L. Zhang, T. Rehfeld, G. Krehl, and A. Seal, "Holistic grid fusion based stop line estimation," in *2020 25th International Conference on Pattern Recognition (ICPR)*. IEEE, 2021, pp. 8400–8407.
- [61] L. Zhang, F. Tafazzoli, G. Krehl, R. Xu, T. Rehfeld, M. Schier, and A. Seal, "Hierarchical road topology learning for urban map-less driving," *arXiv preprint arXiv:2104.00084*, 2021.
- [62] X. L. Tong Tong, Gen Li and Q. Gao, "Image super-resolution using dense skip connections," in *Proc. IEEE Int. Conf. Comput. Vis. (ICCV)*, 2017.
- [63] K. Ding, K. Ma, S. Wang, and E. P. Simoncelli, "Comparison of full-reference image quality models for optimization of image processing systems," *Int. J. Comput. Vis.*, vol. 129, no. 4, pp. 1258–1281, 2021.
- [64] X. Wang, K. Yu, S. Wu, J. Gu, Y. Liu, C. Dong, Y. Qiao, and C. Change Loy, "Esrgan: Enhanced super-resolution generative adversarial networks," in *Proc. Eur. Conf. Comput. Vis. (ECCV)*, 2018, pp. 0–0.
- [65] K. Simonyan and A. Zisserman, "Very deep convolutional networks for large-scale image recognition," *arXiv preprint arXiv:1409.1556*, 2014.
- [66] Y. Jiang, X. Gong, D. Liu, Y. Cheng, C. Fang, X. Shen, J. Yang, P. Zhou, and Z. Wang, "Enlightengan: Deep light enhancement without paired supervision," *IEEE Trans. Image Process.*, vol. 30, pp. 2340–2349, 2021.
- [67] O. Kupyn, V. Budzan, M. Mykhailych, D. Mishkin, and J. Matas, "Deblurgan: Blind motion deblurring using conditional adversarial networks," in *Proc. IEEE Conf. Comput. Vis. Pattern Recognit. (CVPR)*, 2018, pp. 8183–8192.
- [68] R. Zhang, P. Isola, A. A. Efros, E. Shechtman, and O. Wang, "The unreasonable effectiveness of deep features as a perceptual metric," in *Proc. IEEE Conf. Comput. Vis. Pattern Recognit. (CVPR)*, 2018, pp. 586–595.
- [69] K. Ding, K. Ma, S. Wang, and E. P. Simoncelli, "Image quality assessment: Unifying structure and texture similarity," *arXiv preprint arXiv:2004.07728*, 2020.
- [70] E. Agustsson and R. Timofte, "Ntire 2017 challenge on single image super-resolution: Dataset and study," in *Proc. IEEE Conf. Comput. Vis. Pattern Recognit. (CVPR)*, July 2017.
- [71] M. Everingham, S. Eslami, L. Van Gool, C. Williams, J. Winn, and A. Zisserman, "The pascal visual object classes challenge: A retrospective," *Int. J. Comput. Vis.*, vol. 111, 01 2014.
- [72] Z. Wang, A. C. Bovik, H. R. Sheikh, and E. P. Simoncelli, "Image quality assessment: from error visibility to structural similarity," *IEEE Trans. Image Process.*, vol. 13, no. 4, pp. 600–612, 2004.
- [73] R. Zhang, P. Isola, A. A. Efros, E. Shechtman, and O. Wang, "The unreasonable effectiveness of deep features as a perceptual metric," in *Proc. IEEE Conf. Comput. Vis. Pattern Recognit. (CVPR)*, 2018.
- [74] D. Kingma and J. Ba, "Adam: A method for stochastic optimization," *Int. Conf. Learn. Represent. (ICLR)*, 12 2014.
- [75] P. Isola, J.-Y. Zhu, T. Zhou, and A. A. Efros, "Image-to-image translation with conditional adversarial networks," *Proc. IEEE Conf. Comput. Vis. Pattern Recognit. (CVPR)*, 2017.